Few-Body Syst (2023) 64:63
https://doi.org/10.1007/s00601-023-01828-7

Kazuya Aoki · Daichi Arimizu · Sakiko Ashikaga · Wen-Chen Chang · Tatsuya Chujo · Kengo Ebata · Hideto En'yo · Shinichi Esumi · Hideki Hamagaki · Ryotaro Honda · Masaya Ichikawa · Shunsuke Kajikawa · Koki Kanno · Yuta Kimura · Akio Kiyomichi · Takehito K. Kondo · Shono Kyan · Che-Sheng Lin · Chih-Hsun Lin · Yuhei Morino · Hikari Murakami · Tomoki N. Murakami · Ryotaro Muto · Shunnosuke Nagafusa · Wataru Nakai · Satomi Nakasuga · Megumi Naruki · Toshihiro Nonaka · Hiroyuki Noumi · Shuta Ochiai · Kyoichiro Ozawa · Takao Sakaguchi · Hiroyuki Sako · Fuminori Sakuma · Susumu Sato · Shinya Sawada · Michiko Sekimoto · Kenta Shigaki · Kotaro Shirotori · Hitoshi Sugimura · Tomonori N. Takahashi · Yudai Takaura · Ryohei Tatsumi · Kosuke Tsukui · Po-Hung Wang · Kanta Yahiro · Kanako H. Yamaguchi · Satoshi Yokkaichi

Experimental Study of In-medium Spectral Change of Vector Mesons at J-PARC

Received: 23 April 2023 / Accepted: 22 May 2023 / Published online: 11 July 2023

Abstract Chiral symmetry and its spontaneous breaking is an essential property of the QCD vacuum and is closely related to the generation of hadron mass. J-PARC E16 experiment measures dielectron spectra in p+A collisions at 30 GeV to study the in-medium spectral change of vector mesons that signals the partial restoration of the broken symmetry. The experiment uses the primary proton beam available at the high-momentum beam line of the J-PARC hadron experimental facility. We performed three proton-beam runs intended for beamline and detector commissioning. We are preparing for the next commissioning run in 2023 and the first physics run. We present the experimental setup, some of the expected results, preparation status, and some findings in the commissioning runs.

K. Aoki (✉)· R. Honda · Y. Morino · R. Muto · W. Nakai · H. Noumi · K. Ozawa · S. Sawada · M. Sekimoto · H. Sugimura
Institute of Particle and Nuclear Studies (IPNS), High Energy Accelerator Research Organization (KEK), 1-1 Oho, Tsukuba, Ibaraki 305-0801, Japan
E-mail: kazuya.aoki@kek.jp

D. Arimizu · K. Ebata · M. Ichikawa · S. Nagafusa · S. Nakasuga · M. Naruki · S. Ochiai · Y. Takaura · K. Yahiro · K. H. Yamaguchi
Department of Physics, Kyoto University, Kitashirakawa Oiwakecho, Kyoto, Kyoto 606-8502, Japan

S. Ashikaga · H. Noumi · K. Shirotori
Research Center for Nuclear Physics (RCNP), Osaka University, 10-1 Mihogaoka, Ibaraki, Osaka 567-0047, Japan

W.-C. Chang · C.-S. Lin · C.-H. Lin · P.-H. Wang
Institute of Physics, Academia Sinica, Taipei 11529, Taiwan

T. Chujo · S. Esumi · S. Kyan · T. Nonaka · K. Ozawa · K. Tsukui
Center for Integrated Research in Fundamental Science and Engineering, University of Tsukuba, 1-1-1 Tennodai, Tsukuba, Ibaraki 305-8577, Japan

1 Introduction

Although the fundamental theory of strongly interacting particles has been known for many years as quantum chromodynamics (QCD), many aspects of hadrons are yet to be elucidated. The hadron mass is no exception. The properties of a hadron depend on the realized QCD vacuum, and the vacuum itself is a fundamental entity that needs to be investigated. Hadrons in a medium is a playground of QCD and its realization.

The spontaneous breaking of the chiral symmetry in QCD is one of the essential properties and is closely related to the generation of the hadron mass. The chiral condensate $\langle \bar{q}q \rangle$ is an order parameter of the symmetry, and its dependence on temperature and density is discussed, for example, using the NJL model [1]. It suggests that the absolute value of the condensate decreases with increasing temperature and/or density. It predicts threshold behavior at a high temperature. In contrast, it predicts linear dependence on density, and a decrease is expected even at the normal nuclear density. Such a change could result in a measurable difference in hadron properties.

Deeply bound pionic atoms in Sn nuclei were observed, and the isovector parameter b_1 of the pion-nucleus optical potential was deduced to be $b_1 = (-0.1210 \pm 0.0063) m_\pi^{-1}$ [2]. It indicates that the absolute value of the chiral condensate is reduced to $58 \pm 4\%$ in the u and d quark sector at the normal nuclear density.

Another promising way of investigating the hadron mass in a medium is to measure vector meson mass such as ρ, ω, and ϕ by reconstructing invariant mass through e^+e^- decay. The vector mesons decay according to their lifetime. Therefore, the invariant mass distribution is a mixture of decay inside and outside the medium. Since the decay mode has small final state interactions, it is suited for the study. Mesons produced in p+A collisions probe a static finite density system in low temperatures. Among them, we put special emphasis on the ϕ meson because of its narrow width of $\Gamma = 4.2\,\mathrm{MeV}/c^2$ and its isolated peak in contrast to the overlapping ρ and ω mesons. In addition, the ϕ meson in a medium is a good probe of the chiral condensate in the s quark sector [3].

KEK-E325 experiment measured ϕ meson in p+C and Cu collisions at 12 GeV [4]. They reconstructed the invariant mass of e^+e^- pairs. The mass distributions were obtained separately for C and Cu targets and divided into three $\beta\gamma$ groups. They observed an excess on the lower side of the ϕ meson mass peak, only in

H. En'yo · M. Ichikawa · K. Kanno · T. N. Murakami · F. Sakuma · T. N. Takahashi · S. Yokkaichi
RIKEN Nishina Center for Accelerator-Based Science, RIKEN, 2-1 Hirosawa, Wako, Saitama 351-0198, Japan

H. Hamagaki
Institute for Innovative Science and Technology, Nagasaki Institute of Applied Science, 536 Aba-Machi, Nagasaki, Nagasaki 851-0193, Japan

M. Ichikawa · S. Nakasuga · M. Naruki · K.Ozawa · H. Sako · S. Sato
Advanced Science Research Center, Japan Atomic Energy Agency (JAEA), 2-4 Oaza Shirakata, Tokai, Ibaraki 319-1195, Japan

S. Kajikawa
Department of Physics, Tohoku University, Sendai, Miyagi 980-8578, Japan

Y. Kimura · R. Tatsumi
Institute of Physics, Osaka University, Osaka, Japan

A. Kiyomichi
Accelerator Division, Japan Synchrotron Radiation Research Institute (JASRI), 1-1-1 Koto, Sayo, Hyogo 679-5198, Japan

T. K. Kondo · K. Shigaki
Physics Program and International Institute for Sustainability with Knotted Chiral Meta Matter (SKCM2), Hiroshima University, 1-3-1 Kagamiyama, Higashi-Hiroshima, Hiroshima 739-8526, Japan

H. Murakami
Center for Nuclear Study, Graduate School of Science, University of Tokyo, 7-3-1 Hongo, Bunkyoku, Tokyo 113-0033, Japan

T. N. Murakami
Department of Physics, University of Tokyo, 7-3-1 Hongo, Bunkyoku, Tokyo 113-0033, Japan

T. Sakaguchi
Physics Department, Brookhaven National Laboratory, Upton, New York 11973, USA

the case of the Cu targets and $\beta\gamma$ less than 1.25. Analysis was performed under the assumption that mass and width depend linearly on density as,

$$\frac{m(\rho)}{m(0)} = 1 - k_1 \frac{\rho}{\rho_0} \tag{1}$$

$$\frac{\Gamma(\rho)}{\Gamma(0)} = 1 + k_2 \frac{\rho}{\rho_0}, \tag{2}$$

where $m(\rho)$ is the mass of ϕ immersed in nuclear matter at density ρ, $\Gamma(\rho)$ is the width, and ρ_0 is the normal nuclear density. They concluded that $k_1 = 0.034^{+0.006}_{-0.007}$ and $k_2 = 2.6^{+1.8}_{-1.2}$. The conclusion suggests that the mass decreases by 3.4% and the width increases by 3.6 times at the normal nuclear density. Gubler et al. calculated the relation between the ϕ meson mass and the strangeness sigma term σ_s using the QCD sum rule approach [3]. They assumed linear density approximation of the chiral condensate in the s quark sector, $\langle \bar{s}s \rangle_\rho$, as

$$\langle \bar{s}s \rangle_\rho = \langle \bar{s}s \rangle_0 + \langle N|\bar{s}s|N \rangle \rho, \tag{3}$$

$$\sigma_s = m_s \langle N|\bar{s}s|N \rangle. \tag{4}$$

The subscripts ρ and 0 indicate the density of a medium. E325 results and the QCD sum rule calculation suggest a large strangeness sigma term of $\sigma_s = 100$ MeV or even more. In contrast, recent lattice QCD calculations suggest $\sigma_s \sim 50$ MeV [5]. If one takes the Lattice QCD value and the QCD sum rule results, the mass shift should be less than 1 %.

Recently ALICE collaboration studied the p-ϕ interactions by measuring the two-particle correlation function in p+p collisions at LHC [6]. The real part of the scattering length was deduced to be $a = -0.85 \pm 0.34(stat) \pm 0.26(syst)$ fm and an effective range to be $r = 7.85 \pm 1.54(stat) \pm 0.26(syst)$ fm. The properties of ϕ meson in a nuclear medium are closely related to the p-ϕ interactions. One can calculate first-order optical potential [7]

$$V(r) = \frac{1}{2\mu} 4\pi \rho(r) a, \tag{5}$$

where μ is the reduced mass of the proton and the ϕ meson, $\rho(r)$ is the nucleon density evaluated at the distance r, and a is the scattering length. Regarding the potential as the mass reduction of ϕ meson immersed in a nuclear medium, the results indicate a mass reduction of 3.5%, which is similar to the E325 value. HAL QCD collaboration obtained scattering parameters for p and ϕ in the spin 3/2 state [8] using lattice QCD. They deduced a scattering length to be $a^{(3/2)} = -1.43 \pm 0.23(stat)^{+0.36}_{-0.06}(syst)$ fm and an effective range to be $r^{(3/2)} = 2.36 \pm 0.10(stat)^{+0.02}_{-0.48}$ fm at $m_\pi = 146.4$ MeV/c^2. Although the results need extrapolation to physical pion mass to compare with experimental data, the results also suggest a large mass reduction of ϕ mesons in a nuclear medium.

Hartmann et al. studied the production of ϕ mesons in p+A collisions via $\phi \rightarrow K + K-$ at 2.83 GeV at COSY [9]. They measured the momentum-dependent transparency ratio and deduced the in-medium width of the ϕ mesons. The width of the ϕ mesons whose momentum is 1 GeV/c is more than 25 MeV/c^2 and is larger than the E325 results.

A consistent picture has yet to be reached. Therefore, we propose J-PARC E16 [10–12] to give more precise and systematic experimental evidence of spectral change of vector mesons to shed light on the matter.

The paper is organized as follows. In Sect. 2, we introduce the J-PARC E16 spectrometer and its detector components and show some of the expected results for the first and second physics runs. In Sect. 3, we explain the already performed commissioning runs and some of their results. A summary is given in Sect. 4.

2 J-PARC E16 experiment

J-PARC E16 experiment has been proposed to measure vector mesons ρ, ω, and ϕ via e^+e^- decay in p+A collisions at 30 GeV [10]. The spectra are a mixture of decay inside and outside the nucleus, therefore, they are sensitive to the in-medium spectral change. The decay channel is a clean probe with small final state interactions. Disadvantages are the small branching ratios of the order of 10^{-4} and the thin experimental targets to suppress spectrum distortion and combinatorial backgrounds. The J-PARC E16 experiment overcomes the difficulties by using a high-intensity proton beam and a large acceptance spectrometer. It adopts the same

Table 1 E16 Experimental targets

Target	A	Thickness	Rad. length	Int. length	Quantity
C	12.0	500 μm	0.21%	0.10%	1
Cu	63.5	80 μm	0.55%	0.052%	2

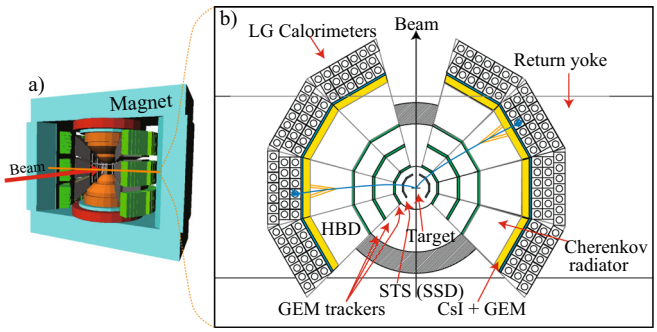

Fig. 1 J-PARC E16 spectrometer.**a** 3D image of the spectrometer. Spectrometer components are built inside a magnet. **b** Plan view of the E16 spectrometer

concept as KEK-E325 but collects much more statistics with a better mass resolution to provide a systematic study. The expected mass resolution is 5.8 MeV/c^2 for ϕ meson whose $\beta\gamma$ is less than 0.5, while the measured mass resolution was 10.7 MeV/c^2 for E325 [4]. The beam intensity is ten times higher, and the acceptance is roughly five times larger compared to KEK-E325.

It uses the primary proton beam available at the high-momentum beamline in the hadron experimental facility at J-PARC [13]. A 30 GeV proton beam is provided by the J-PARC Main Ring (MR) and is slowly extracted and delivered through the switching yard (SY) to the hadron experimental facility. A tiny fraction ($\sim 10^{-4}$) of the proton beam is separated by a Lambertson magnet at SY and delivered to the high-momentum beamline and its experimental area where the J-PARC E16 spectrometer is located. The rest of the beam is provided for other experiments. The Lambertson magnet is a dipole magnet associated with a field-free hole and they are separated with a thin magnet yoke. Most of the proton beam enters into the field-free hole and goes straight for the other experiments. The rest of the beam that enters the dipole part of the magnet changes the trajectory to the high-momentum beam line. The beam intensity of the high-momentum beamline is 1×10^{10} protons per 2-sec spill duration with a repetition cycle of 5.2 sec.

The experimental targets used for the first physics run are summarized in Table 1. Targets are chosen to have an interaction length of 0.1% in total, and a target foil to have a radiation length of 0.5% or less. Restriction on the radiation length is to suppress spectral distortion due to energy loss in the target material, and to suppress combinatorial background due to conversion electrons. Therefore, a C target and two Cu targets were chosen and they are arranged in series.

2.1 Experimental setup

Figure 1a) displays a 3D image of the E16 spectrometer which is built inside a large dipole magnet. The magnetic field is about 1.8 T at maximum. Figure 1b) shows a plan view of the spectrometer. The proton beam is delivered from bottom to top, bombarding the targets at the spectrometer center. The spectrometer comprises a silicon tracking system (STS), three layers of Gas electron multiplier TRackers (GTR), Hadron Blind Cherenkov detectors (HBD), and Lead-Glass electromagnetic calorimeters (LG). The first two detectors are tracking devices to precisely determine the particle trajectories in the magnetic field for momentum measurement. The rest of the detectors are for electron identification. A set of these detectors that covers 30 degrees horizontally and vertically is called a module. In Fig. 1, eight modules are visible, which is our intermediate goal of the detector configuration for the first physics run. To cope with the 10 MHz interaction expected at the experimental targets, we utilize silicon detectors and gas electron multipliers (GEM) [14].

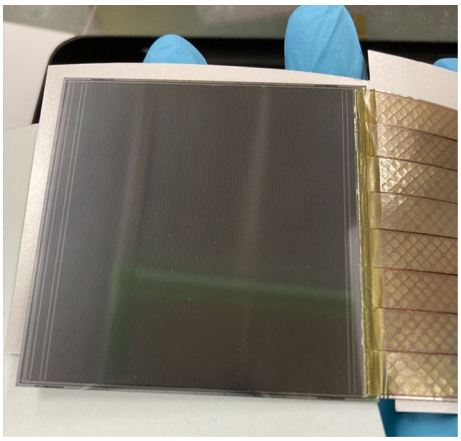

Fig. 2 Photo of a prototype STS sensor. Mirco-cables are tab-bonded on the electrodes of the sensor for signal readout

2.1.1 STS

The innermost tracking device of the J-PARC E16 spectrometer is a silicon detector. Fine segmentation and good timing resolution are essential for high-rate capability, high mass resolution, and background reduction. The used silicon strip detectors (SSD) were borrowed from the J-PARC E03 group for the first three commissioning runs. However, reproduction is difficult and they also have thick and large frames. Therefore, we developed a new SSD in collaboration with the GSI-CBM group called the silicon tracking system (STS) [15].

Figure 2 is a photo of the silicon sensor made by Hamamatsu Photonics [16]. The sensitive area is 60 mm $\times$ 60 mm, and its thickness is 320 μm. The sensor is double-sided, and the strip pitch is 58 μm. The strips on the n side are sensitive to the bending direction of charged particles. The strips on the p side are tilted by 7.5 degrees, making the two-dimensional position reconstruction possible. Position resolution of 30 μm and timing resolution of 6 nsec is expected.

Figure 3 depicts the mechanical design of the STS. Ten sensors are prepared for the next commissioning run and the first physics run, Run 0d and Run 1 (see Sec. 2.2). and they are arranged so that they surround the experimental targets which are located at the center. The sensors are mounted on eight carbon fiber ladders. The sensor signals are delivered by micro-cables to Front End Board-8 (FEB8) and processed.

The module assembly is done at GSI in Germany and will be delivered to Japan. Four out of ten sets of sensor-cables-FEB8 were assembled at the time of presentation.[1]

2.1.2 GTR

Three layers of GEM Trackers (GTRs), GTR1, GTR2, and GTR3 are located at distances of approximately $R = 200, 400,$ and 600 mm from the center, respectively. The sensitive areas are 100×100 mm^2, 200×200 mm^2, and 300 $\times$ 300 mm^2 respectively. Each GTR chamber comprises a mesh electrode, three GEM foils, and a two-dimensional strip readout. Ar+CO2(30%) is used as an amplification gas. Incident charged particles ionize the gas between the mesh electrode and the top GEM. The ionized electrons are then multiplied by the three GEM foils, and induced charges on the strips are read out. The x- and y-strips are perpendicular, and the strip pitch is 350 μm and 1400 μm, respectively. The x-strips are sensitive to the bending direction of charged particles. The resolution in x-direction is 100 μm to achieve the required mass resolution. Each chamber is mounted on a carbon fiber frame to reduce the material budget around the sensitive area.

2.1.3 HBD

The Hadron blind detector (HBD) [17,18] is a Cherenkov detector used to identify electrons from pions. It was developed for the E16 experiment based on the PHENIX HBD [19]. It is a CF_4 filled chamber whose inner bottom surface is covered by a photocathode made of GEM. The gas serves both as a Cherenkov radiator and

[1] In Mar. 2023, the module assembly and delivery to Japan were completed. The construction of the support structure shown in Fig. 3 and the purchase of necessary electronics components were also completed.

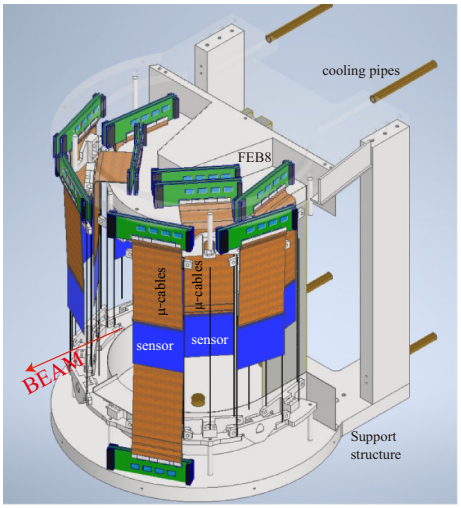

Fig. 3 Mechanical design of the STS. Ten sensors are mounted on eight carbon-fiber ladders. The signals are delivered through micro-cables to Front End Board-8 (FEB8)

an amplification gas. The Cherenkov threshold is 4.0 GeV/c for pions. The length of the radiator is 500 mm, and 11 photoelectrons are expected.

The photocathode comprises a mesh electrode, three GEM foils, and a hexagonal pad readout. The top GEM is gold-plated, on top of which CsI is evaporated. The Cherenkov light that is emitted by an incident electron is converted into photoelectrons by the CsI layer. They are then amplified by the three GEM foils, and the induced charge on pads is read out. A charged particle whose velocity is below the Cherenkov threshold does ionize the gas between the mesh electrode and the top GEM. However, signals due to such ionized electrons are largely suppressed by applying a reverse bias so that the ionized electrons drift to the mesh electrode and are absorbed in. This way, the detector is blind to hadrons. The sensitive area of the GEM foils is $300\times300\,\mathrm{mm}^2$ and an HBD module comprises four GEM stacks.

The oxygen and water contamination of the gas should be at the order of ppm because they absorb ultraviolet light, and reduce the Cherenkov signals. A gas-purifier integrated recirculation system was developed to save the expensive CF_4 gas. The readout pad, whose side is 10 mm, is smaller than the size of the Cherenkov blob, whose size is 34 mm in diameter. Therefore, the cluster size can be used to increase the rejection factor. A pion rejection factor of 98% is expected while keeping an electron efficiency of 68%.

2.1.4 LG

The LG is used to identify electrons from pions [20]. An LG module comprises 38 lead-glass blocks. Each block is associated with a fine-mesh photomultiplier. An incident electron induces an electromagnetic shower and Cherenkov light from the shower is detected by the photomultiplier while an incident pion has less probability of producing a shower leaving a smaller signal. The lead glass of the TOPAZ experiment [21] was reshaped and used for the E16 experiment. It has eight times the radiation length in depth. The fine-mesh photomultiplier tube is Hamamatsu R6683. A pion rejection factor of 90% is expected while maintaining an efficiency of 90% for 0.4 GeV electrons.

2.2 Staging approach

We adopt a staging approach; the run plan is summarized in Table 2. Three commissioning runs were already performed in 2020 and 2021. They are called Run 0a, 0b, and 0c. The acceptance was gradually increased and it fulfills the intermediate goal of an 8-module configuration as depicted in Fig. 4 for Run 0d and Run 1. Run 0d is the next commissioning run scheduled in 2023, and Run 1 is the first physics run. PAC approval was granted for Run 0d but has yet to be for Run 1. It has to be requested based on the outcome of Run 0d.

Table 2 E16 Run Plan

Run	Year	User Time	Targets	Configuration SSD+GTR+ HBD+LG
Run 0a	Jun. 2020	159 hrs	C, Cu	6+6+4+6
Run 0b	Feb. 2021	110 hrs	C, Cu	6+8+6+6
Run 0c	May. 2021	134 hrs	C, Cu	6+8+6+6
Run 0d	2023	100 hrs	C, Cu	$10+10^{2}$+8+8
Run 1	TBD	1280 hrs	C, Cu	$10+10^{2}$+8+8
Run 2	TBD	2560 hrs	C, Cu, Pb, CH_2	26+26+26+26

[2] Two GTR modules are only equipped with GTR1 and GTR2

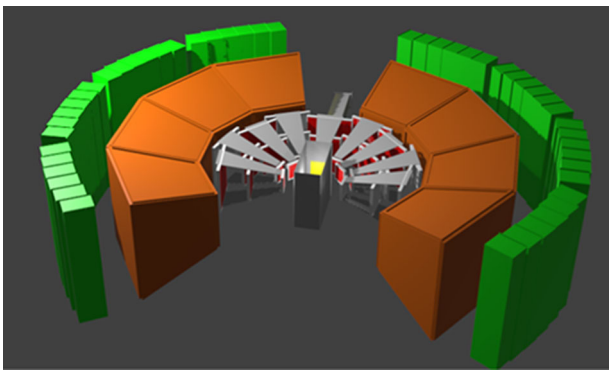

Fig. 4 E16 Run1 configuration

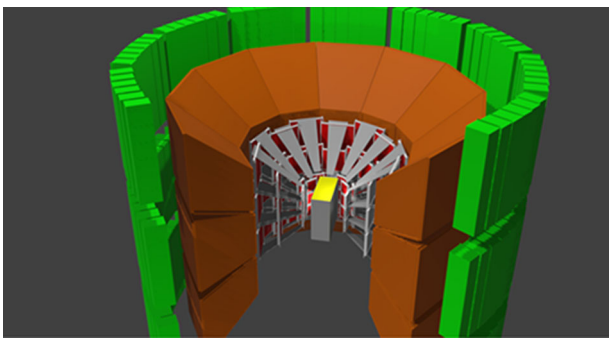

Fig. 5 E16 Run2 configuration

Later, more modules are added to the upper and lower sides of the 8-module configuration and finally, 26 modules are built as depicted in Fig. 5 for Run 2, the second physics run. An additional budget should be acquired to build the Run 2 configuration.

Figure 6 displays a photo of the spectrometer which was taken in 2020 before Run 0a.

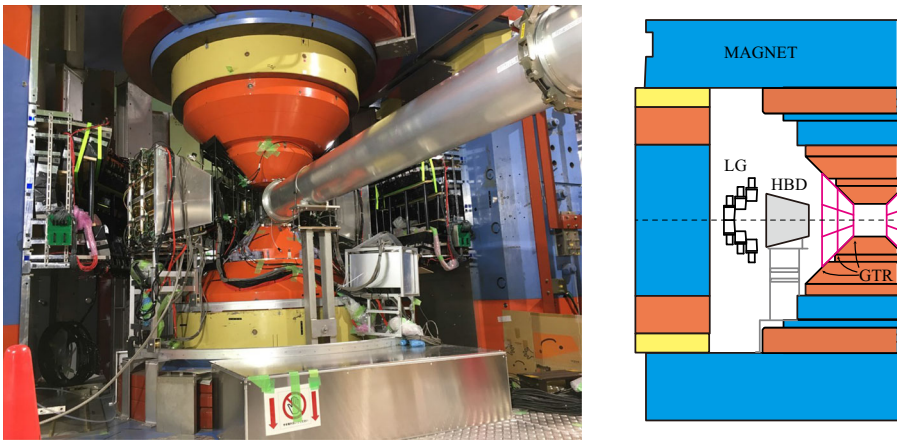

Fig. 6 Left: Photograph of the E16 spectrometer that was taken in 2020. Right: Illustration of some of the installed detector components. SSDs and targets are not visible in the picture

2.3 Expected results

2.3.1 Run1 expectation

A simulation was performed to evaluate sensitivity to the spectral change. Momentum distribution of the vector mesons was obtained using an event generator JAM [22]. Breit-Wigner shape was used for the mass distribution, and E325-type in-medium spectral change was assumed. The mass and the width of ϕ mesons were determined according to Eq. 1. Woods-Saxon-type nuclear density distribution was assumed. Internal radiative corrections were applied using PHOTOS [23]. The detector response was simulated using GEANT4 [24].

Figure 7 displays the mass distributions expected results in Run 1. They are divided into four $\beta\gamma$ bins of the ϕ meson. The red line shows the expected line shape when ϕ meson vacuum shape is assumed. Black points are expected when the E325-type model was assumed. The expected data points are fitted with the expected vacuum shape and an exponential background. The upper four plots are obtained when the whole area was used for the fit, while the lower four plots are obtained when the region between the green lines is eliminated from the fit. The area indicated by the green lines is where the samples of modified mass are expected. All $\beta\gamma$ bins are expected to be significant in contrast to the case of E325, where only the mass distribution for the slowest $\beta\gamma$ bin was significant. In total, 15 k ϕ mesons are expected to be collected in Run1.

An excess fraction is defined as $\frac{N_{\rm excess}}{N_\phi + N_{\rm excess}}$ where N_ϕ is the number of ϕ mesons in the vacuum shape and $N_{\rm excess}$ denotes the number of excess. The excess is plotted in Fig. 8 against the $\beta\gamma$ of ϕ mesons. The tendency becomes clearer and more significant, confirming the picture that slower-moving ϕ mesons in the larger target have the larger excess fraction. Such a clear tendency would be stronger evidence for in-medium modification of spectral functions.

In addition, the dispersion relation, that is, the momentum dependence of the mass, in a medium can be measured for the first time for hadrons. Figure 9 displays the expected results with statistics 1.7 times the Run1. They are plotted with a theoretical calculation based on the QCD sum rule [25,26]. The calculation applies only up to 1 GeV/c but is extrapolated to guide the eye. Recently, Kim et al. extended the validity up to 3 GeV/c by calculating higher-order terms [27]. Dispersion relation itself is an important property of a pseudo-particle. It can also be used to extrapolate the mass to zero momentum, where most of the QCD sum rule calculations are done. These calculations predict not only a momentum dependence but also a polarization dependence. Measurement of polarization-dependent hadron mass is discussed in [28].

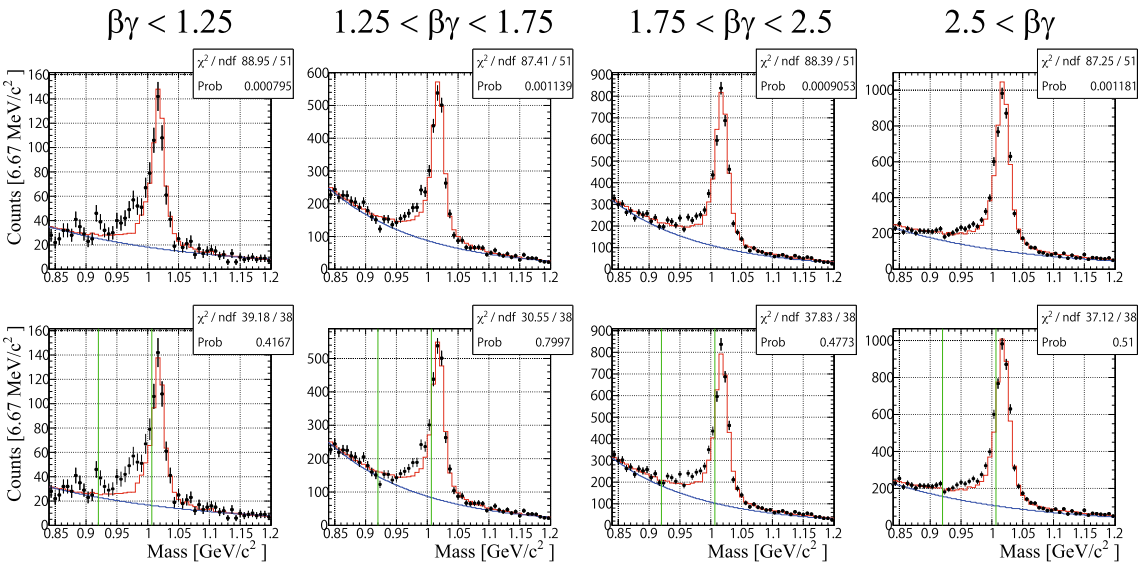

Fig. 7 Invariant mass distributions expected in Run1. The plots are divided into four samples according to $\beta\gamma$ of the e^+e^- pairs. Black points are expected in Run 1. Red lines show the expected line shape assuming the vacuum shape. The upper four panels are obtained when the data is fitted for the entire region, while the lower four panels are obtained when the area between the green lines is eliminated from the fit [11]

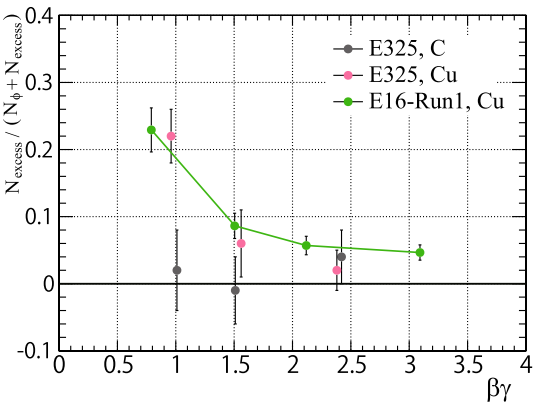

Fig. 8 Excess fraction vs $\beta\gamma$ of ϕ mesons. Black (pink) points are the E325 results for the C (Cu) target. Green points are the expected results in Run1 [11]

2.3.2 Run 2 expectation

In Run 2, we plan to use Pb targets, where ϕ has a higher probability of in-medium decay than in the Cu targets. By selecting very slowly moving ϕ mesons whose $\beta\gamma$ is less than 0.5, and using the heavy target, double peak such as Fig. 10 is expected (the plot was made without combinatorial background). Such a double-peak structure is clear and robust evidence of in-medium modification.

3 Commissioning runs

We have performed three commissioning runs, Run 0a, 0b, and 0c. They were intended for the beamline and the detector commissioning.

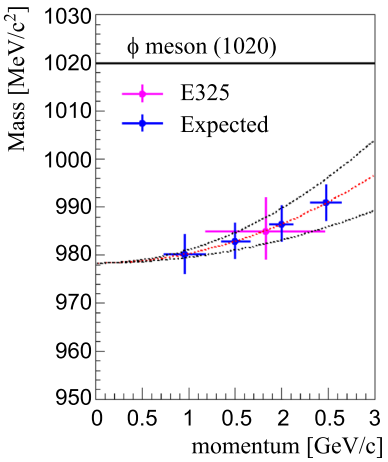

Fig. 9 Dispersion relation. Pink point is the E325 results. Blue points show the expected sensitivity when 1.7 times Run 1 statistics are collected. Dotted lines indicate a theoretical prediction extrapolated to guide the eye [11]

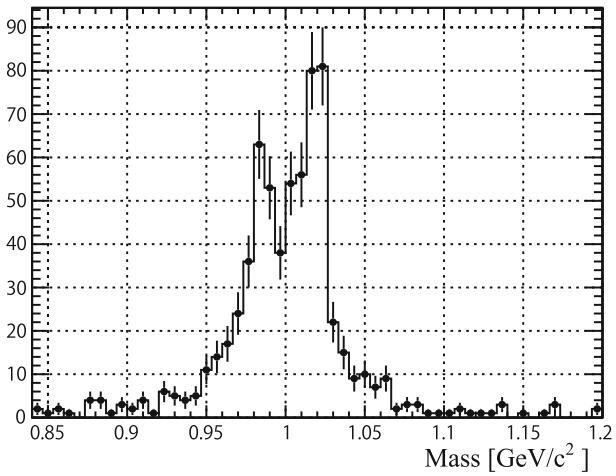

Fig. 10 E16 Run 2 expectation with Pb target and selection of very slowly moving ϕ mesons [12]

3.1 Beamline commissioning

During the runs, the beam quality was studied and improved. The beam loss was minimized by adjusting the beam optics to reduce the background from the scattered beam particles. The beam loss was measured using scintillators and proportional counters placed along the beamline.

The beam profile was measured, and the widths were typically 1.3 mm horizontally and 0.4 mm vertically. To measure the beam profile, copper rods with a width of 300 um were placed horizontally and vertically at the center of the spectrometer instead of the experimental target. The scattering rates were monitored by varying the beam position horizontally and vertically.

Sometimes a spill ten times more intense than the setting was delivered during Run 0a. Such a beam cannot be accepted because it would be out of the rate capability of the data acquisition system (DAQ), and it could damage the detectors when intensity was set to the design value of 1×10^{10} protons per spill. Such an anomalous beam was suppressed by accelerator tuning and never experienced again. The bulk time structure in a spill was tamed by introducing a time-dependent current-adjustment system of the beamline magnets.

Although there were many improvements in the beam quality, a beam micro-structure remained. A highly time-concentrated beam was delivered every 5 msec and 5.2 μsec. It resulted in a very low DAQ live rate of about 15%, while the expectation was 75%. The structure made trigger requests more often during the DAQ dead time than the random trigger assumption. It also enhances fake triggers due to overlapping events.

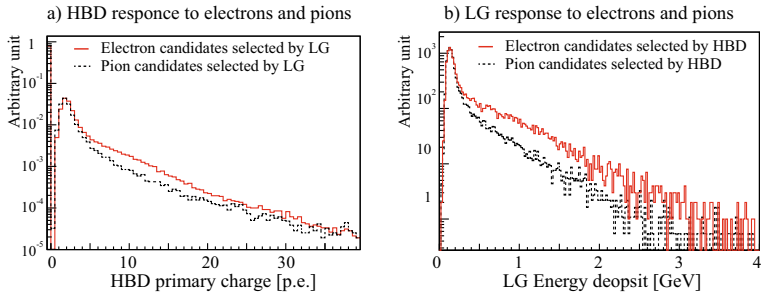

Fig. 11 **a** HBD Primary charge distribution for the electron and pion data samples that the LG selects. **b** LG Energy deposit distribution for the electron and pion data samples that the HBD selects. See [20] for a detailed description

Several upgrades of the accelerator and the E16 experiment are expected to mitigate the situation. The new magnet power supplies that replaced the old ones of the Main Ring (MR) are known to have smaller ripples for frequencies that match the 5 msec structure. New beam transport optics remove position-momentum correlation at the Lambertson-type magnet, suppressing the beam-momentum-dependent time structure. The E16 DAQ will be upgraded to make the dead time shorter. All these upgrades are expected to improve the situation. It will be tested during Run 0d.

3.2 Detector commissioning

Detector commissioning was done using the proton beam. Here we present the performance of the electron identification detectors of the spectrometer. The performance of the HBD was evaluated using the electron and pion candidates that the LG selects and vice versa.

Figure 11a displays the primary charge distribution measured by the HBD for the electron (red) and pion (black) samples that the LG selects. A clear enhancement can be seen for electron candidates, suggesting that the HBD successfully observes Cherenkov light from the incident electrons. Figure 11b shows the energy deposit measured by the LG for the electron (red) and pion (blue) samples that the HBD selects. LG also sees a clear enhancement for electron samples. See [20] for a detailed description.

4 Summary

J-PARC E16 measures dielectron in p+A collisions at 30 GeV to study the origin of hadron mass through the spectral change of vector mesons in a nuclear medium. Many experiments and theoretical efforts related to the topic already exist, and new results are also emerging, bringing renewed interest to the topic. We gradually increased the acceptance and reached an intermediate goal for the first physics run. It is one-third of the design configuration for the second physics run. We have performed three commissioning runs. The beam was studied and tuned, and the detectors were operated and tested. The beam quality was significantly improved, but a micro-structure remained that degraded data acquisition efficiency. It is expected to be mitigated by the accelerator and the detector upgrades. We will perform another commissioning run, Run 0d, test the upgraded beam quality, and commission the spectrometer with newly added detector components and the improved data acquisition system.

Acknowledgements We express our gratitude to the J-PARC hadron beamline group for constructing and operating the high-momentum beamline at the hadron experimental facility. We appreciate the support of the staff at KEKCC, RIKEN-CCJ, and RIKEN HOKUSAI. We wish to thank the KEK electronics system group for their support in developing and operating the read-out electronics. We also would like to express our gratitude to the LEPS2 and K1.8 groups for providing their electronics and Drs. K. Tanida and S.H. Hayakawa for delivering support for the old SSD data taking. We must express sincere appreciation to the CBM-STS team for their effort in developing and constructing STS for the E16 experiment. The author would like to thank S.H. Lee and P. Gubler for the fruitful discussions. This work was supported by the RIKEN SPDR program, Grant-in-Aid for JSPS Fellows JP18J20494, MEXT/JSPS KAKENHI grant Nos. JP19654036, JP19340075, JP21105004, JP26247048, JP15H05449, JP15K17669, JP18H05235, JP20H 01935, JP20H05647 and JP21H01102, and the Ministry of Science and Technology of Taiwan grant No. MOST108-2112-M-001-020.

Author contributions K. Aoki wrote the manuscript text and prepared figures 1-6. W. Nakai and K. A. prepared figures 7-8, and 10. S. Yokkaichi and K. A. prepared figure 9. K. Kannno, S. Nakasuga and K. A. prepared figure 11. All authors reviewed the manuscript.

Declarations

Conflict of interest The authors declare that they have no conflict of interest.

References

1. M.F.M. Lutz, S. Klimt, W. Weise, Meson properties at finite temperature and baryon density. Nucl. Phys. A **542**, 521–558 (1992). https://doi.org/10.1016/0375-9474(92)90256-J
2. T. Nishi, et al. Pionic atom unveils hidden structure of QCD vacuum (2022) arXiv:2204.05568 [nucl-ex]. https://doi.org/10.1038/s41567-023-02001-x
3. P. Gubler, K. Ohtani, Constraining the strangeness content of the nucleon by measuring the ϕ meson mass shift in nuclear matter. Phys. Rev. D 90(9), 094002 (2014) arXiv:1404.7701 [hep-ph]. https://doi.org/10.1103/PhysRevD.90.094002
4. R. Muto, et al. Evidence for in-medium modification of the phi meson at normal nuclear density. Phys. Rev. Lett. 98, 042501 (2007) arXiv:nucl-ex/0511019. https://doi.org/10.1103/PhysRevLett.98.042501
5. Y. Aoki, et al. FLAG Review 2021. Eur. Phys. J. C 82(10), 869 (2022) arXiv:2111.09849 [hep-lat]. https://doi.org/10.1140/epjc/s10052-022-10536-1
6. S. Acharya, et al. Experimental Evidence for an Attractive p-ϕ Interaction. Phys. Rev. Lett. 127(17), 172301 (2021) arXiv:2105.05578 [nucl-ex]. https://doi.org/10.1103/PhysRevLett.127.172301
7. V.A. Baskov, J.P. Bocquet, V. Kouznetsov, A. Lleres, A.I. L'vov, L.N. Pavlyuchenko, V.V. Polyanski, D. Rebrevend, G.A. Sokol, Possibility to study eta mesic nuclei and photoproduction of slow eta mesons at the GRAAL facility (2003) arXiv:nucl-ex/0306011
8. Lyu, Y., Doi, T., Hatsuda, T., Ikeda, Y., Meng, J., Sasaki, K., Sugiura, T.: Attractive N-ϕ interaction and two-pion tail from lattice QCD near physical point. Phys. Rev. D 106(7), 074507 (2022) arXiv:2205.10544 [hep-lat]. https://doi.org/10.1103/PhysRevD.106.074507
9. Hartmann, M., et al.: Momentum dependence of the phi-meson nuclear transparency. Phys. Rev. C 85, 035206 (2012) arXiv:1201.3517 [nucl-ex]. https://doi.org/10.1103/PhysRevC.85.035206
10. Yokkaichi, S., et al.: Proposal - Electron pair spectrometer at the J-PARC 50-GeV PS to explore the chiral symmetry restoration in QCD (2006). https://ribf.riken.jp/~yokkaich/E16/pub/proposal.pdf
11. S. Ashikaga et al., Measurement of vector meson mass in nuclear matter at J-PARC. JPS Conf. Proc. **26**, 024005 (2019). https://doi.org/10.7566/JPSCP.26.024005
12. K. Ozawa et al., Towards the measurement of the mass modifications of vector mesons in a finite density matter. Acta Phys. Polon. A **142**(3), 399–404 (2022). https://doi.org/10.12693/APhysPolA.142.399
13. E. Hirose et al., Construction of new branching point and operation of new primary beam line at the J-PARC hadron facility. IEEE Trans. Appl. Supercond. **32**(6), 4101904 (2022). https://doi.org/10.1109/TASC.2022.3168525
14. F. Sauli, GEM: a new concept for electron amplification in gas detectors. Nucl. Instrum. Meth. A **386**, 531–534 (1997). https://doi.org/10.1016/S0168-9002(96)01172-2
15. Heuser, J., et al.: Technical design report for CBM - silicon tracking system (STS). GSI Report (2013). https://repository.gsi.de/record/54798/files/GSI-Report-2013-4.pdf
16. Hamamatsu photonics. https://www.hamamatsu.com
17. Tserruya, I., Aoki, K., Woody, C.: Hadron blind Cherenkov counters. Nucl. Instrum. Meth. A 970, 163765 (2020) arXiv:2003.12858 [physics.ins-det]. https://doi.org/10.1016/j.nima.2020.163765
18. K. Kanno et al., Development of a hadron blind detector using a finely segmented pad readout. Nucl. Instrum. Meth. A **819**, 20–24 (2016). https://doi.org/10.1016/j.nima.2016.02.063
19. Anderson, W., et al.: Design, Construction, Operation and Performance of a Hadron Blind Detector for the PHENIX Experiment. Nucl. Instrum. Meth. A 646, 35–58 (2011) arXiv:1103.4277 [physics.ins-det]. https://doi.org/10.1016/j.nima.2011.04.015
20. S. Nakasuga et al., Commissioning of the electron identification system for Dilepton measurement in pA collisions at J-PARC. Nucl. Instrum. Meth. A **1041**, 167335 (2022). https://doi.org/10.1016/j.nima.2022.167335
21. S. Kawabata, R. Sugahara, T. Tauchi, N. Ujiie, Y. Watanabe, S. Kuroda, T. Suwada, TOPAZ barrel electromagnetic calorimeter. Nucl. Instrum. Meth. A **270**, 11 (1988). https://doi.org/10.1016/0168-9002(88)90004-6
22. Nara, Y., Otuka, N., Ohnishi, A., Niita, K., Chiba, S.: Study of relativistic nuclear collisions at AGS energies from p + Be to Au + Au with hadronic cascade model. Phys. Rev. C 61, 024901 (2000) arXiv:nucl-th/9904059. https://doi.org/10.1103/PhysRevC.61.024901
23. Davidson, N., Przedzinski, T., Was, Z.: PHOTOS interface in C++: Technical and Physics Documentation. Comput. Phys. Commun. 199, 86–101 (2016) arXiv:1011.0937 [hep-ph]. https://doi.org/10.1016/j.cpc.2015.09.013

24. S. Agostinelli et al., GEANT4-a simulation toolkit. Nucl. Instrum. Meth. A **506**, 250–303 (2003). https://doi.org/10.1016/S0168-9002(03)01368-8
25. Lee, S.H.: Vector mesons in-medium with finite three momentum. Phys. Rev. C 57, 927–930 (1998) arXiv:nucl-th/9705048. https://doi.org/10.1103/PhysRevC.57.927. [Erratum: Phys.Rev.C 58, 3771 (1998)]
26. Lee, S.H.: Vector mesons in dense matter. Nucl. Phys. A 670, 119–126 (2000) arXiv:nucl-th/9904007. https://doi.org/10.1016/S0375-9474(00)00081-6
27. Kim, H., Gubler, P.: The ϕ meson with finite momentum in a dense medium. Phys. Lett. B 805, 135412 (2020) arXiv:1911.08737 [hep-ph]. https://doi.org/10.1016/j.physletb.2020.135412
28. Park, I.W., Sako, H., Aoki, K., Gubler, P., Lee, S.H.: Disentangling longitudinal and transverse modes of the ϕ meson through dilepton and kaon decays. Phys. Rev. D 107(7), 074033 (2023) arXiv:2211.16949[hep-ph]. https://doi.org/10.1103/PhysRevD.107.074033